Paleo-heat flows, radioactive heat generation, and the cooling and deformation history of Mercury

Javier Ruiz [a,*], Valle López [b], Isabel Egea-González [c]

[a] Departamento de Geodinámica, Facultad de Ciencias Geológicas, Universidad Complutense de Madrid, 28040 Madrid, Spain

[b] Escuela Técnica Superior de Ingenieros en Topografía, Geodesia y Cartografía, Universidad Politécnica de Madrid, Carretera de Valencia, km 7.5, 28031 Madrid, Spain

[c] Instituto de Astrofísica de Andalucía, CSIC, Glorieta de la Astronomía s/n, 18008 Granada, Spain

* Corresponding author. E-mail: jaruiz@geo.ucm.es (J. Ruiz)

Abstract

Estimates of lithospheric strength for Mercury, based on the depth of thrust faults associated with large lobate scarps (which were most probably formed previously to ~3 Ga) or on the effective elastic thickness of the lithosphere supporting a broad rise in the northern smooth plains (whose formation is poorly constrained, but posterior to 3.8 Ga), serve as a basis for the calculation of paleo-heat flows, referred to the time when these structures were formed. The so-obtained paleo-heat flows can give information on the Urey ratio (*Ur*), the ratio between the total radioactive heat production and the total surface heat loss. By imposing the condition $Ur < 1$ (corresponding to a cooling Mercury, consistent with the observed widespread contraction), we obtain an upper limit of 0.4 times the average surface value for the abundance of heat-producing elements in the outer solid shell of Mercury. We also find that if the formation of the northern rise occurred in a time posterior to ~3 Ga, then in that time the Urey ratio was lower, and the cooling more intense, than when most of large lobate scarps were formed. Thus, because largest lobate scarps deform older terrains (suggesting more intense contraction early in the mercurian history), we conclude that the northern rise was formed previously to 3 Ga. If the age of other smooth plains large wavelength deformations is similar, then tectonic activity in Mercury would have been limited in the last three billion of years.

Key words: Mercury; Mercury, interior; Tectonics; Thermal histories.

1. Introduction

Calculation of paleo-heat flows from lithospheric strength (using as strength indicator the depth of large thrust faults or the effective elastic thickness of the lithosphere)

can potentially be used in order to constrain the thermal evolution of a planetary body (e.g., Ruiz et al., 2011), because the obtained values refer to the time of deformation (i.e., the time of faulting or loading). In the case of Mercury, paleo-heat flows calculated in this way could be useful for obtaining information on the cooling history of Mercury and their geological implications. Paleo-heat flows can also be used to constrain the whole abundance of radioactive heat-producing elements (HPE) in the silicate portion of Mercury independently of specific compositional models.

The surface of Mercury exhibits numerous compressional tectonic features (e.g., Strom et al., 1975; Dzurisin, 1978; Watters et al., 2001, 2009), most probably related to planetary cooling and contraction (e.g., Strom et al., 1975). The more representative of these structures are lobate scarps, interpreted to be the surface expression of large thrust faults deforming the lithosphere down to depths of 30 or 40 km (Watters et al., 2002; Ritzer et al., 2010; Egea-González et al., 2012). Most of the large lobate scarps were probably formed during the first third of the history of the planet, because they affect mainly Calorian or older terrains (Watters et al., 2009; Watters and Nimmo, 2010), although some lobate scarps affect Mansurian or Kuiperian terrains (Banks et al., 2012). Previous works have used the deduced estimates of depth of faults beneath lobate scarps, taken as representative of the brittle-ductile transition (BDT) depth, in order to calculate the local heat flow at the time when faulting occurred (Watters et al., 2002; Nimmo and Watters, 2004; Egea-González et al., 2012).

Recently, the existence of a broad, ~950 km in diameter, topographic rise in the northern plains of Mercury (Figure 1) has been revealed through MESSENGER topography (Zuber et al., 2012); moreover, a high (~70-90 km) effective elastic thickness has been

derived, from MESSENGER topography and gravity, for the lithosphere supporting this rise (Smith et al., 2012). The surface appearance of the northern rise is similar to that observed across the northern plains (Figure 2), and flooded craters around this rise have floors tilted consistently with regional slopes, suggesting that the northern plains were elevated here after their emplacement (Balcerski et al., 2012; Dickson et al., 2012); the time of loading of the lithosphere by the northern rise is therefore not well constrained. Similar observations have been reported for other volcanic plains, implying that large-scale topographic modifications postdated volcanic plains emplacement at 3.7-3.8 Ga (Solomon et al., 2012). Heat flows have not been calculated previously from the effective elastic thickness of the lithosphere in the northern rise, although they would give complementary information to those obtained for other regions from fault depths.

In this work, we first use heat flows derived from the BDT depth beneath lobate scarps and HPE surface abundances in order to constrain the total abundance of heat sources in the silicate fraction of Mercury. Next, we use our results for lobate scarps to constrain the calculation of paleo-heat flows from the effective elastic thickness of the lithosphere in the northern rise. Finally, we will discuss the implications of our results for the cooling history of Mercury and for the timing of large-scale topography modifications of the Calorian volcanic plains.

2. Heat flows and HPE abundance from the depth of thrust faults

Faulting depths of thrust faults associated with lobate scarps have been estimated in several cases through forward modeling procedures by using topographic profiles derived from stereoscopic Mariner 10 images (Watters et al., 2002, Nimmo and Watters, 2004),

MESSENGER Laser Altimeter flyby data (Ritzer et al., 2010), or Earth-based radar surveys (Egea-González et al., 2012). In all the cases the obtained faulting depths are similar. These faulting depths can in turn be used to derive heat flows, because large faults usually deform the lithosphere down to the crustal brittle-ductile transition (BDT), which is temperature-dependent.

Here we take as representative the case of thrust faults in the Kuiper region (including Santa Maria Rupes and two unnamed lobate scarps; Figures 1 and 3), studied by Egea-González et al. (2012), in order to calculate heat flows following the methodology described in Ruiz et al. (2009). We therefore use a BDT depth between 30 and 40 km, a surface gravity of 3.7 m s^{-2}, a surface temperature of 435 K (representative for the Kuiper region; see Vasavada et al., 1999; Aharonson et al., 2004), strain rates of 10^{-16} s^{-1} and 10^{-19} s^{-1} (which are typical values for, respectively, active terrestrial plate interiors (e.g., Tesauro et al., 2007) and for planetary thermal contraction (Schubert et al., 1988)), and the flow law of dry Maryland diabase for dislocation creep parameters (Mackwell et al., 1998). Heat flows are calculated from the temperature at the BDT depth; this temperature is obtained by equating brittle (pressure-dependent) and ductile (temperature-dependent) strength at the BDT depth. For consistency with the crustal model of Smith et al. (2012) we assume a crustal density of 3100 kg m^{-3}. We assume crustal potassium, thorium and uranium abundances (1150 ppm, 220 ppb and 90 ppb, respectively), based on surface values determined by MESSENGER GRS measurements (Peplowski, et al., 2011). Surface measurements can be considered as roughly representative for the crust, due to the heavy mixing caused by impact cratering (for the case of Mars see, for example, Taylor et al., 2006). The HPE abundances are converted to heat dissipation rates by using standard decay

constants (e.g., Van Schmus, 1995), and a temporal range of 3.0-4.0 Ga, roughly corresponding to Tolstojan and Calorian times (Spudis and Guest, 1988; Tanaka and Hartmann, 2008), the time when most of large lobate scarps would have been formed (Watters et al., 2009; Watters and Nimmo, 2010). Finally, we use a thermal conductivity of 2 W m^{-1} K^{-1} for the entire crust, a value appropriate for intact, non-porous, basaltic rocks (e.g., Beardsmore and Cull, 2001). For descriptions of the construction of temperature profiles and of the calculations of heat flows from the BDT depth see, respectively, Appendixes A and B; the value of the used constant are shown in Table D1.

The obtained heat flows are between 18 and 29 mW m^{-2}, consistent with previous results (Watters et al., 2002; Nimmo and Watters, 2004; Egea-González et al., 2012). Smith et al. (2012) have found substantial crustal thickness variations on Mercury, which should have an influence on the geographical pattern of heat flow, due to differences in heat production between crust and mantle. The Kuiper region has a crust ~20 km thicker than average. Assuming that crustal HPE are homogeneously distributed, a constant sublithosphere heat flow (which is reasonable if the mantle is sluggishly convective, or not convective in all; Breuer et al., 2007; Redmond and King, 2007), and, in this point of the calculations, zero HPE in the lithospheric mantle (defined as the portion of the upper mantle capable of support stresses during geological periods of time), the results for the Kuiper region can be scaled to global average heat flow values between 15 and 25 mW m^{-2}.

Our results can be used to obtain constrains on the total concentration of heat sources in the silicate portion of the planet. The existence of a solid, thin (410 ± 37 km) and dense (3650 ± 225 kg m^{-3}), shell overlying Mercury's core has been inferred from

MESSENGER gravity measurements and Earth-based determinations of axis orientation (Smith et al., 2012). Because its high density, this outer solid shell could include, besides the crust and mantle, a solid FeS layer atop the core (Smith et al., 2012). In this case, the silicate layer (crust plus mantle), where radioactive heat production occurs, would be thinner than the outer solid shell.

In a cooling planet (as evidenced by the ubiquitous contraction observed in Mercury) the ratio between the total radioactive heat production and the total surface heat loss, know as Urey ratio and denoted by *Ur*, must be lower than 1. Heat flows derived from the BDT depth can therefore be used to calculate the Urey ratio as a function of the heat production in the solid outer shell of Mercury. Thus, Figure 4 shows Urey ratios as a function of the ratio (referred here to as Γ) between the average heat production in the solid outer shell (which is here characterized by mean thickness and density values derived by Smith et al. (2012)) and the average surface heat production. In other words, Γ = 1 implies a uniform HPE distribution in the crust and mantle equivalent to the value observed at the surface and lower Γ values imply decreasing concentrations of HPE at depth (or in the mantle). If a solid FeS layer atop the core is assumed (or finally demonstrated) to exist, then the silicate layer must be thinner than the outer solid shell, and Γ can accordingly be scaled to the proportion of heat sources in the silicate portion of the planet.

Figure 4 presents the results obtained using local and crustal thickness-scaled surface heat flows as representative for Mercury global averages. We only show cases producing lower (upper) limits for the Urey ratio, which correspond to slower (faster) strain rate and older (younger) times (and not to extreme values of surface heat flow). The results show that the Urey ratio increases, for a given time and strain rate, as a function of Γ.

Imposing the condition $Ur < 1$ (implying interior cooling), an upper limit around 0.4 is obtained for Γ. However, through this procedure is not possible to find a lower limit for Γ, because it is not easy to put a lower limit for *Ur*.

3. Heat flows from the effective elastic thickness of the lithosphere in the northern rise: implications for formation time

The thick elastic lithosphere supporting the northern rise of Mercury provides an independent opportunity to calculate paleo-heat flows, as well as Urey ratios as a function of Γ that can be compared with equivalent estimates based on the BDT depth of thrust faults associated with lobate scarps.

Smith et al. (2012) found that the effective elastic thickness of the lithosphere (T_e) in the northern rise is weakly dependent on the mean thickness of the crust (b), and obtained best fit values ranging from T_e = 70 km for b = 100 km to T_e = 90 km for b = 25 km; these authors obtained T_e = 80 km for their preferred crustal thickness of 50 km, and a similar value should be derived for b = 75 km, as it is possible to be deduced from their Figure S7. Effective elastic thicknesses can be converted to estimates of heat flow following the equivalent strength envelope procedure (McNutt, 1984; Ruiz et al., 2011). Here we calculate surface heat flows for the northern rise (for the pairs of T_e and b values above indicated) by assuming zero lithospheric curvature (the lithosphere beneath the northern rise is almost unflexed (Smith el al., 2012)) and taking into account the possibility of mechanical decoupling between crust and lithospheric mantle (see Appendix C).

For the crust, we use thermal and mechanical parameters as in Section 2. For the upper mantle, we use the flow law for dislocation creep of dry olivine (Chopra and

Paterson, 1984), and a temperature-dependent thermal conductivity appropriate for forsterite olivine (McKenzie et al., 2005), which is useful for an iron-poor mantle, as apparently is the case of Mercury (Nittler et al., 2011). We use a surface temperature of 275 K, appropriate for the location (centered around 68ºN, 33ºE) of the northern rise (see Vasavada et al., 1999; Aharonson et al., 2004), and strain rates of 10^{-16} and 10^{-19} s^{-1}. See Appendix A for calculation of temperature profiles, and Appendix D for the used parameters.

The amount of heat sources in the lithospheric mantle of Mercury is unknown. As extreme cases we use 0 and 0.4 times the surface abundance of HPE, and a density of 3300 kg m^{-3} by consistency with Smith et al. (2012) and an iron-poor upper mantle. The value of 0.4 is based on the upper limit obtained for Γ in the previous section. If the solid outer shell includes a basal FeS layer, then Γ should be re-scaled to a value somewhat higher than 0.4 (see previous section). However, the outer solid shell also includes the crust, which should be enriched in HPE. Therefore, HPE average abundances in the non-crustal portion of the outer solid shell should be somewhat lower than 0.4 times the average surface value to offset the crustal contribution. Thus, we consider this value as a reasonable upper limit for the heat production in the lithospheric mantle.

On the other hand, as above mentioned, the timing of uplift of the northern rise is poorly constrained (Dickson et al., 2012), although it is most probably younger than the emplacement of the northern smooth plains (which is dated in ~3.7-3.8 Ga; Head et al., 2011). This uncertainty affects the calculation of radioactive heat production rates, and hence the derivation of surface heat flows, although its influence is relatively moderated (Figure 5). For example, we obtain surface heat flows ranging from 24-33 mW m^{-2} for 3.8

Ga (taken as an upper limit for the age of northern rise formation), and 18-28 mW m^{-2} for the current time. Thus, the total heat flow range is 18-33 mW m^{-2}, although the absence of a clear temporal constraint for the northern rise uplift limits the significance of these values.

Heat flows obtained for the northern rise region can be used to calculate Urey ratios as a function of Γ in a way similar to that described in Section 2. Because this region has a crust ~15 km thinner than average, we scale local heat flows for the mean crustal thickness by taking into account the difference in radioactive heat production between crust and mantle (for the cases with mantle HPE abundances equal to 0 and 0.4 times the surface value). Urey ratios are calculated, as a function of Γ, from the so-corrected global average heat flows. (The so-obtained Urey ratios are hereafter referred as NR-based; similarly, Urey ratios derived from global average heat flows based on the BDT depth below lobate scarps are hereafter referred as LS-based.)

Figure 6 shows upper and lower limits of NR-based Urey ratios calculated for 3.7-3.8 Ga, the time of smooth plains emplacement. These upper and lower limits have the same dependence on strain rate and time as Urey ratios derived in the previous section. By comparison, Figure 6 also shows LS-based Urey ratios calculated by taking into account mantle HPE abundances equal to 0 and 0.4 times the average surface value (which has the effect of decreasing *Ur* lower limits with respect to those shown in Figure 4). The NR-based *Ur* range is within the LS-based range, although in the lower portion. Figure 6 also shows NS-based Urey ratios calculated for a loading time of 3.0 Ga. In this case, NS-based Urey ratios overlap with LS-based values only for a narrow range, corresponding to the uppermost (lowermost) part of NR (LS)-based Urey ratios. For loading times younger than 2.7 Ga, there is no overlap at all between NS- and LS-based Urey ratios. This signifies that

if the formation of the northern rise topography occurred in a time more recent than ~3 Ga, then in that time the Urey ratio was lower, and the cooling more intense, than when most of large lobate scarps were formed. This contradicts the observation that the largest lobate scarps deform older terrains, suggesting more intense contraction and cooling early in the mercurian history (Hauck et al., 2004). Thus, the northern rise most likely formed previously to 3 Ga.

Several evidences suggest a significant presence of volatiles in Mercury (e.g., Kerber et al., 2011; Nittler et al., 2011). If wet rheologies (Caristan, 1982; Chopra and Paterson, 1984) are used for the crust and/or the mantle lithosphere, then the obtained heat flows are accordingly decreased. This reduction is lower for the case of the northern rise (because the relatively stronger lithospheric mantle contributes more to the strength, and from here to the effective elastic thickness, of the lithosphere) than for the case of lobate scarps in the Kuiper region (because mantle rheology does not affect the results here). This implies lower Urey ratios for the northern rise with respect to those for the Kuiper region, and there is no overlap between the Urey ratios deduced for both regions. This in turn implies that wet rheologies are not relevant for the lithosphere of Mercury, which is in accordance with predictions of BDT depth and effective elastic thickness from the thermal evolutions models of Williams et al. (2011).

4. Implications for the cooling and deformation history of Mercury

The calculation of Urey ratios from surface heat flows (in turn based on estimates of lithospheric strength and adequately scaled to derive global average values), serves to obtain information on both HPE abundances and timing of large-scale deformation on

Mercury.

The upper limit here deduced for average HPE abundances in the outer solid shell, although rough, is consistent with predictions of heat production from most compositional models (see Hauck et al., 2004; Peplowski et al., 2011). Lamentably, we are unable to obtain a lower limit, which does not permit more precise conclusions in this respect.

There is evidence for changes in long wavelength topography postdating the emplacement of Calorian smooth plains (Balcerski et al., 2012; Dickson et al., 2012; Solomon et al., 2012; Zuber et al., 2012), including the northern rise and a quasi-linear, roughly WSW-ENE oriented, ridge that deforms mid-latitude mercurian surfaces and affects the Caloris basin interior (Zuber et al., 2012). The timing of this widespread large-scale deformation is not clear. However, we have obtained Urey ratios (as a function of the abundance of HPE in the solid outer shell), that suggest that the formation of the northern rise should have occurred early, in some moment within the time range of formation of most of large lobate scarps, and hence when thermal contraction of Mercury was more intense. The timing of other long wavelength smooth plains deformation could be similar. In this case contraction and tectonic deformation (including large-scale folding and thrust faulting) would have been much more limited after the Calorian. Some lobate scarps continued to be formed in Mansurian and Kuiperian times (Banks et al., 2012), including very young small-scale lobate scarps, but they most probably were witnesses of an already greatly reduced geological activity in Mercury.

Acknowledgements

We thank the useful comments and suggestions from Scott King and an anonymous reviewer. JR work was supported by a contract Ramón y Cajal co-financed from the Ministerio de Economía y Competitividad of Spain and the European Social Fund.

Appendix A. Temperature profiles

Temperature profiles in the crust are calculated by assuming a homogeneous distribution of radioactive heat sources. Also, we use a constant thermal conductivity for the entire crust, and therefore the temperature at a given depth z is given by

$$T_z = T_s + \frac{Fz}{k_c} - \frac{\rho_c H_c z^2}{2k_c}, \quad \text{(A1)}$$

where T_s is the surface temperature, F is the surface heat flow, k_c is the thermal conductivity of the crust, ρ_c is the density of the crust, and H_c is the crustal heat production rate per unit mass. We use T_s = 435 K, representative for the Kuiper region, (see Vasavada et al., 1999; Aharonson et al., 2004), and k_c = 2 W m^{-1} K^{-1}, a value appropriate for intact, non-porous, basaltic rocks (see, for example, Beardsmore and Cull, 2001). We assume crustal potassium, thorium and uranium abundances (1150 ppm, 220 ppb and 90 ppb, respectively), based on surface average values measured by MESSENGER GRS measurements (Peplowski, et al., 2011). These abundances are converted to heat dissipation rates by using standard decay constants (e.g., Van Schmus, 1995).

Temperature profiles in the upper mantle are calculated by assuming a temperature-

dependent thermal conductivity appropriate for forsterite olivine, which is useful for an iron-poor mantle, and therefore

$$\frac{dT}{dz} = \frac{F_{cb} - \rho_m H_m (z - b_c)}{k_m(T)}, \tag{A2}$$

where $F_{cb} = F - \rho_c H_c b_c$ is the heat flow at the base of the crust, ρ_m and H_m are, respectively, the density and heat production rate per mass unity of the mantle lithosphere, b_c is the crustal thickness, and k_m is the thermal conductivity of the lithospheric mantle. For k_m we use (McKenzie et al., 2005)

$$k_m = \frac{a}{1 + c(T - 273)} + \sum_{i=0}^{3} d_i T^i, \tag{A3}$$

where $a = 5.3$, $c = 0.0015$, $d_0 = 1.753 \times 10^{-2}$, $d_1 = -1.0364 \times 10^{-4}$, $d_2 = 2.2451 \times 10^{-7}$ and $d_3 = -3.4071 \times 10^{-11}$.

Appendix B. Heat flows from the depth of the brittle-ductile transition

The depth of the brittle-ductile transition (BDT) can be used in order to calculate surface heat flows (Ruiz and Tejero, 2000), which are derived from the temperature T_{BDT} at the BDT depth. The brittle strength, in absence of pore pressure, is calculated according to the expression (e.g., Ranalli, 1997)

$$(\sigma_1 - \sigma_3)_b = \alpha g \rho_c z \,, \tag{B1}$$

where α is a coefficient depending on the stress regime (which is 3 for pure compression; e.g., Ranalli, 1997), and g is the acceleration due to the gravity (3.7 m s^{-2} for Mercury). The ductile strength (which does not depend on the stress regime) is given by

$$(\sigma_1 - \sigma_3)_d = \left(\frac{\dot{e}}{A}\right)^{1/n} \exp\left(\frac{Q}{nRT}\right), \tag{B2}$$

where $\dot{e}$ is the strain rate, A, Q, and n are laboratory-determined constants, R (= 8.31446 J mol^{-1} K^{-1}) is the gas constant, and T is the absolute temperature. The temperature at the BDT depth is therefore obtained by equating the brittle and ductile strength for the depth z = z_{BDT},

$$T_{BDT} = \frac{Q}{R}\left[\ln \frac{A(\alpha g \rho_c z_{BDT})^n}{\dot{e}}\right]^{-1}; \tag{B3}$$

the heat flow is then obtained from

$$F = \frac{k_c (T_{BDT} - T_s)}{z_{BDT}} + \frac{z_{BDT} \rho_c H}{2}. \tag{B4}$$

Appendix C. Heat flows from the effective elastic thickness of the lithosphere

The effective elastic thickness is a measure of the total strength of the lithosphere, integrating contributions from brittle and ductile layers and from elastic cores of the lithosphere (for a review see Watts and Burov, 2003). Effective elastic thickness estimates can be converted to heat flows following the equivalent strength envelope procedure described by McNutt (1984). This methodology is based on the condition that the bending moment of the mechanical lithosphere must be equal to the bending moment of the equivalent elastic layer of thickness T_e.

If lithospheric curvature due to flexure is small (as in the case of the northern rise of Mercury), it can be neglected: for the case with mechanically welded crust and lithospheric mantle T_e is equal to the depth to the base of the mechanical lithosphere, which is defined as the depth at which the ductile strength reaches a low value of 10 MPa (see Ranalli, 1994; Ruiz et al., 2006) and below which there are no further significant increases in strength. Equation (B2), applied to lithospheric mantle rocks, can be used to obtain the temperature corresponding to a ductile strength of 10 MPa, and the surface heat flow is then obtained by matching this temperature to a thermal profile derived simultaneously solving equations (A1) y (A2).

If the strength at the base of the crust is lower than 10 MPa the lithosphere is considered rheologically stratified, with mechanically decoupled crust and lithospheric mantle, and the total effective elastic thickness is given by (Burov and Diament, 1992)

$$T_e = \left(t_{ec}^3 + t_{em}^3\right)^{1/3}, \qquad \text{(C1)}$$

where t_{ec} and t_{em} are, respectively, the mechanical thicknesses of the crust and the mantle lithosphere, defined as the part of the crust or lithospheric mantle above the depth at which the ductile strength decreases to 10 MPa. In this case, the surface heat flow is obtained by calculating the thermal profile that satisfies the condition imposed by equation (C1).

Appendix D. Parameters

The values of the used constant are summarized in Table D1.

References

Aharonson, O., Zuber, M. T., Solomon, S. C., 2004. Crustal remanence in an internally magnetized non-uniform shell: a possible source for Mercury's magnetic field? Earth and Planet. Sci. Lett., 218, 261–268.

Balcerski, J.A., et al., 2012. Tilted crater floors: recording the history of Mercury's long-wavelength deformation. Lunar Planet. Sci. Conf. 43st. Abstract 1850.

Banks, M.E., et al., 2012. Stratigraphic relationships between lobate scarps and young impact craters on Mercury: implications for the duration of lobate scarp formation. Lunar Planet. Sci. Conf. 43st. Abstract 2684.

Beardsmore, G.R., Cull, J.P., 2001. Crustal heat flow. A guide to measurement and modelling, Cambridge Univ. Press, Cambridge, 324 pp.

Breuer, D., Hauck, S.A., Buske, M., Pauer, M., Spohn, T., 2007. Interior evolution of Mercury. Spce Sci. Rev. 132, 229–260.

Burov, E.B., Diament, M., 1992. Flexure of the continental lithosphere with multilayered

rheology. Geophys. J. Int. 109, 449-468.

Caristan, Y., 1982. The transitions from high temperature creep to fracture in Marylan diabase. J. Geophys. Res. 87, 6781-6790.

Chopra, P.N., Paterson, M.S., 1984. The role of water in the deformation of dunite. J. Geophys. Res. 89, 7861-7876.

Dickson, J.L., et al., 2012. Topographic rise in the northern smooth plains of Mercury: characteristics from MESSENGER image and altimetry data and candidate modes of origin. Lunar Planet. Sci. Conf. 43st. Abstract 2249.

Dzurisin, D., 1978. The tectonic and volcanic history of Mercury as inferred from studies of scarps, ridges, throughs and other lineaments. J. Geophys. Res. 83, 4883-4906.

Egea-González, I., Ruiz, J., Fernández, C., Williams, J.-P., Márquez, A., Lara, L.M., 2012. Depth of thrust faulting and ancient heat flows in the Kuiper region of Mercury from lobate scarp topography. Planet. Spa. Sci. 60, 193-198.

Hauck, S.A., Dombard, A.J., Phillips, R.J., Solomon, S.C., 2004. Internal and tectonic evolution of Mercury. Earth Planet. Sci. Lett. 222, 713-728.

Head, J.W., et al., 2011. Flood volcanism in the northern high latitudes of Mercury revealed by MESSENGER. Science 333, 1853-1856.

Kerber, L., Head, J.W., Solomon, S.C., Murchie, S.L., Blewett, D.T., Wilson, L., 2009. Explosive volcanic eruptions on Mercury: Eruption conditions, magma volatile content, and implications for interior volatile abundances. Earth Planet. Sci. Lett., 285, 263–271.

Mackwell, S.J., Zimmerman, M.E., Kohlstedt, D.L., 1998. High-temperature deformation of dry diabase with application to tectonics on Venus. J. Geophys. Res. 103, 975-984.

McKenzie, D., Jackson, J., Priestley, K., 2005. Thermal structure of oceanic and continental lithosphere. Earth Planet. Sci. Lett. 233, 337-349.

McNutt, M.K., 1984. Lithospheric flexure and thermal anomalies. J. Geophys. Res. 89, 11,180-11,194.

Nimmo, F., Watters, T.R., 2004. Depth of faulting on Mercury: implications for heat flux and crustal and effective elastic thickness. Geophys. Res. Lett., 31, L02701, doi:10.1029/2003GL018847.

Nittler, L.R., et al., 2011. The Major-Element Composition of Mercury's Surface from MESSENGER X-ray Spectrometry. Science 333, 1847-1850.

Peplowski, P.N., et al., 2011. Radioactive elements on Mercury’s surface from MESSENGER: implications for the planet’s formation and evolution. Science 333, 1850-1852.

Ranalli, G., 1994. Nonlinear flexure and equivalent mechanical thickness of the lithosphere. Tectonophysics 240, 107-114.

Ranalli, G., 1997. Rheology of the lithosphere in space and time. Geol. Soc. Spec. Pub. 121, 19-37.

Redmond, H.L., King, S.D., 2007. Does mantle convection currently exist on Mercury? Phys. Earth Planet. Inter. 164, 221-231.

Ritzer, J.A., Hauck, S.A., Barnouin, O.S., Solomon, S.C., Watters, T.R., 2010. Mechanical Structure of Mercury's Lithosphere from MESSENGER Observations of Lobate Scarps. Lunar Planet. Sci. Conf. 41st. Abstract 1533.

Ruiz, J., Tejero, R., 2000. Heat flows through the ice lithosphere of Europa. J. Geophys. Res. 105, 23,283-23,289.

Ruiz, J., McGovern, P.J., Tejero, R., 2006. The early thermal and magnetic state of the cratered highlands of Mars. Earth Planet. Sci. Lett. 241, 2-10.

Ruiz, J., Williams, J.P., Dohm, J.M., Fernández, C., López V., 2009. Ancient heat flow and crustal thickness at Warrego rise, Thaumasia highlands, Mars: Implications for a stratified crust. Icarus 203, 47-57.

Ruiz, J., et al., 2011. The thermal evolution of Mars as constrained by paleo-heat flows, Icarus 215, 508-517.

Schubert, G., Ross, M.N., Stevenson, D.J., Spohn, T., 1988. Mercury's thermal history and the generation of its magnetic field. In: Vilas, F., Chapman C.R., Matthews M.S. (Eds.), Mercury. Univ. of Arizona Press, Tucson, pp 429-460.

Smith, D.E., et al., 2012. Gravity field and internal structure of Mercury from MESSENGER. Science 336, 214-217.

Solomon, S.C., et al., 2012. Long-wavelength topography change on Mercury: evidence and mechanism. Lunar Planet. Sci. Conf. 43st. Abstract 1578.

Spudis, P.D., Guest, J.E., 1988. Stratigraphy and geologic history of Mercury. In: Vilas, F., Chapman, C.R., Matthews, M.S. (Eds.), Mercury. Univ. Arizona Press, Tucson, pp 118-164.

Strom, R. G., Trask, N. J., Guest, J. E., 1975. Tectonism and volcanism on Mercury. J. Geophys. Res. 80, 2478-2507.

Schubert, G., Ross, M.N., Stevenson, D.J., Spohn, T., 1988. Mercury's thermal history and the generation of its magnetic field. In: Vilas, F., Chapman C.R., Matthews M.S. (Eds.), Mercury. Univ. of Arizona Press, Tucson, pp 429-460.

Tanaka, K.P., Hartmann, W.K., 2008. The planetary timescale. In: Ogg, J.G., Ogg, G.M.,

Gradsteim, F.M. (Eds.), The Concise Geologic Time Scale. Cambridge Univ. Press, New York, pp. 13-22.

Taylor, G.J., et al., 2006. Bulk composition and early differentiation of Mars. J. Geophys. Res. 111, E03S10, doi:10.1029/2005JE002645. [Printed 112(E3), 2007]

Tesauro, M, Kaban, M. K., Cloetingh, S. A. P. L., Hardebol, N. J., Beekman, F., 2007. 3D strength and gravity anomalies of the European lithosphere. Earth and Planet. Sci. Lett. 263, 56-73.

Van Schmus, W.R., 1995. Natural radioactivity of the crust and mantle. In: Ahrens, T.J. (Ed.), Global Earth physics: A handbook of physical constants. AGU Reference Shelf 1, American Geophysical Union, Washington, D.C., pp. 283-291.

Vasavada, A. R., Paige, D. A., Wood, S. E., 1999. Near-surface temperatures on Mercury and the Moon and the stability of polar ice deposits. Icarus 141, 179-193.

Watters, T.R., Nimmo, F., 2010. The tectonics of Mercury. In: Watters, T.R., Schultz, R.A. (Eds.), Planetary Tectonics. Cambridge Univ. Press. Cambridge, pp 15-80.

Watters, T.R., Cook, A.C., Robinson, M.S., 2001. Large-scale lobate scarps in the southern hemisphere of Mercury. Planet. Spa. Sci. 49, 1523-1530.

Watters, T.R., Schultz, R.A., Robinson, M.S., Cook, A.C., 2002. The mechanical and thermal structure of Mercury´s early lithosphere. Geophys. Res. Lett. 29, 10.1029/2001GL014308.

Watters, T.R., Solomon, S.C., Robinson, M.S., Head, J.W., André, S.L., Hauck, S.A., Murchie, S.L., 2009. The tectonics of Mercury: The view after MESSENGER's first flyby. Earth and Planet. Sci. Lett. 285, 283-296.

Watts, A.B., Burov, E.B, 2003. Lithospheric strength and its relation to the elastic and

seismogenetic layer thickness. Earth Planet. Sci. Lett. 213, 113-131.

Williams, J.P., Ruiz, J., Rosenburg, M.A., Aharonson, O., Phillips, R.J., 2011. Solar insolation driven variations of Mercury's lithospheric strength. J. Geophys. Res., 116, E01008, doi: 10.1029/2010JE003655.

Zuber, M.T., et al., 2012. Topography of the northern hemisphere of Mercury from MESSENGER laser altimetry. Science 336, 217-220.

Figure caption

Figure 1. Globe map of Mercury showing the location of the Kuiper region and the Northern rise.

Figure 2. MESSENGER mosaic showing a large extension of smooth plains, including the northern rise, whose approximate center is indicated by NR. The surface geology at the northern rise is non differentiable of that of surrounding plains. Moreover, its central area is affected by several arcuate wrinkle ridges (white arrows), whose orientation pattern seem unrelated to the rise (but maybe related to a buried impact basin). Thus, surface geology suggests that the formation of the northern rise postdates plains emplacement.

Figure 3. Mariner 10 image showing large lobate scarps in the Kuiper region, which include Santa Maria Rupes and two unnamed scarps, provisionally dubbed SK_3 and SK_4. Faulting depths of ~30-40 km obtained from Earth-based radar topography profiles (Egea-González et al., 2012) are similar to those derived for lobate scarps in other regions from stereoscopic Mariner 10 images or MESSENGER Laser Altimeter flyby data, and for that reason are taken in this study as representative for Mercury.

Figure 4. Upper and lower limits to the Urey ratio as a function of the average abundance of HPE at the outer solid shell of Mercury per mass unit (for the surface value, $\Gamma = 1$). LS indicates heat flow values estimated from the depth of faulting beneath lobate scarps. “Local” refers to calculations performed using heat flow values directly derived from faulting depths in the Kuiper region, whereas “global” refers to calculations performed by scaling these heat flow values to account for regional crustal thickness (and hence heat production) variations. See text for further details.

Figure 5. Surface heat flow estimated from the effective elastic thickness of the lithosphere supporting the northern rise as a function of loading age. “Local” refers here to calculations performed using heat flow values obtained for the northern rise Kuiper region, whereas “global” refers to calculations performed by scaling these heat flow values to account for regional crustal thickness (and hence heat production) variations.

Figure 6. Upper and lower limits to the Urey ratio as a function of the average abundance, per mass unit, of HPE at the outer solid shell of Mercury (for the surface value, $\Gamma = 1$). LS and NS indicate, respectively, values obtained by using heat flows derived from the faulting depths beneath lobate (scaled for global average crustal thickness) and from the effective elastic thickness of the lithosphere at the northern rise region. Upper and lower limit age calculations use mantle lithosphere HPE abundances equal to 0 and 0.4 times, respectively, the surface value, which have the effect of widening the *Ur* range for a given value of Γ.

Table D1. Parameters used in the calculations (see text for further explanations).

Parameter	**Value and Units**
Surface temperature, T_s	
Kuiper Region	435 K
Northern Rise	275 K
Crust thermal conductivity, k_c	2 W m^{-1} K^{-1}
Lithospheric mantle thermal conductivity, k_m	k_m (T), see Appendix A
HPE abundances in the crust	
K	1150 ppm
Th	220 ppb
U	90 ppb
Crustal density, ρ_c	3100 kg m^{-3}
Mantle density, ρ_m	3300 kg m^{-3}
Stress-related parameter for compression, α	3
Surface gravity, g	3.7 m s^{-2}
Strain rate, $\dot{e}$	10^{-16} s^{-1} - 10^{-19} s^{-1}
Crustal rheology	
A	8 MPa^{-n} s^{-1}
n	4.7
Q	485 kJ mol^{-1}
Lithospheric mantle rheology	
A	28840 MPa^{-n} s^{-1}
n	3.6
Q	535 kJ mol^{-1}
Gas constant, R	8.31446 J mol^{-1} K^{-1}

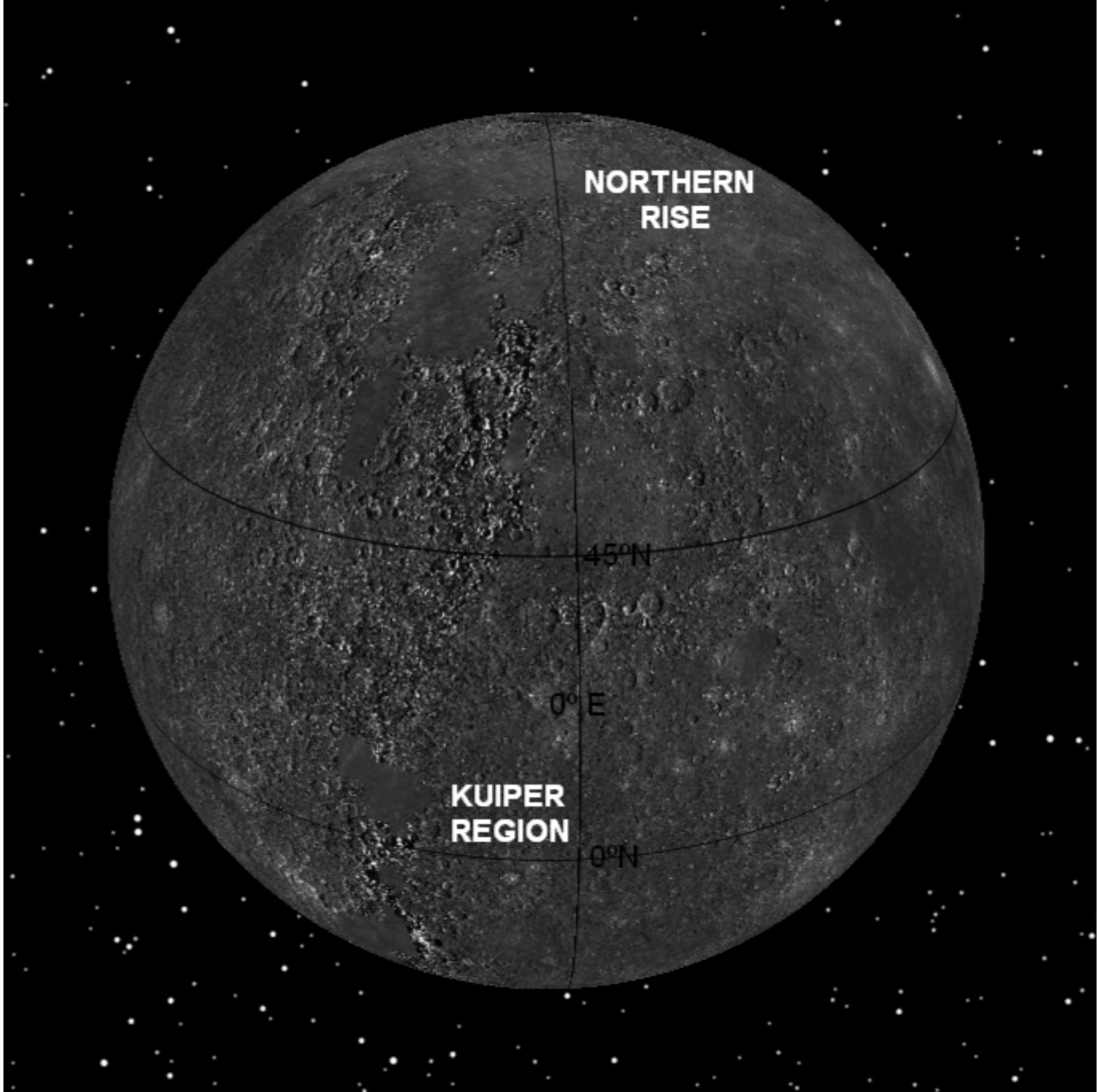
NORTHERN
RISE
45°N
0° E
KUIPER
REGION
0°N

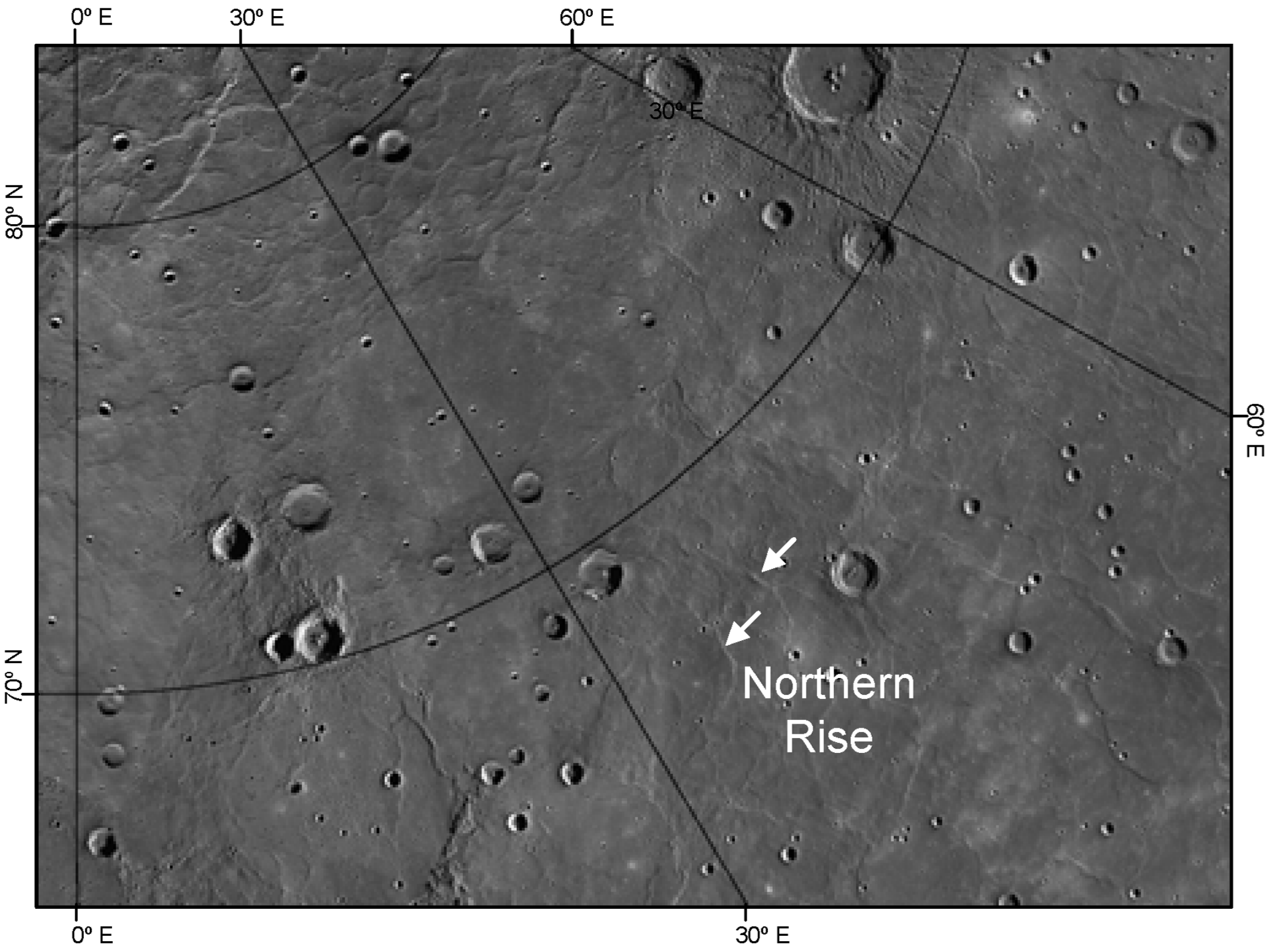
0º E
30º E
60º E
30º E
80º N
60º E
70º N
Northern
Rise
0º E
30º E

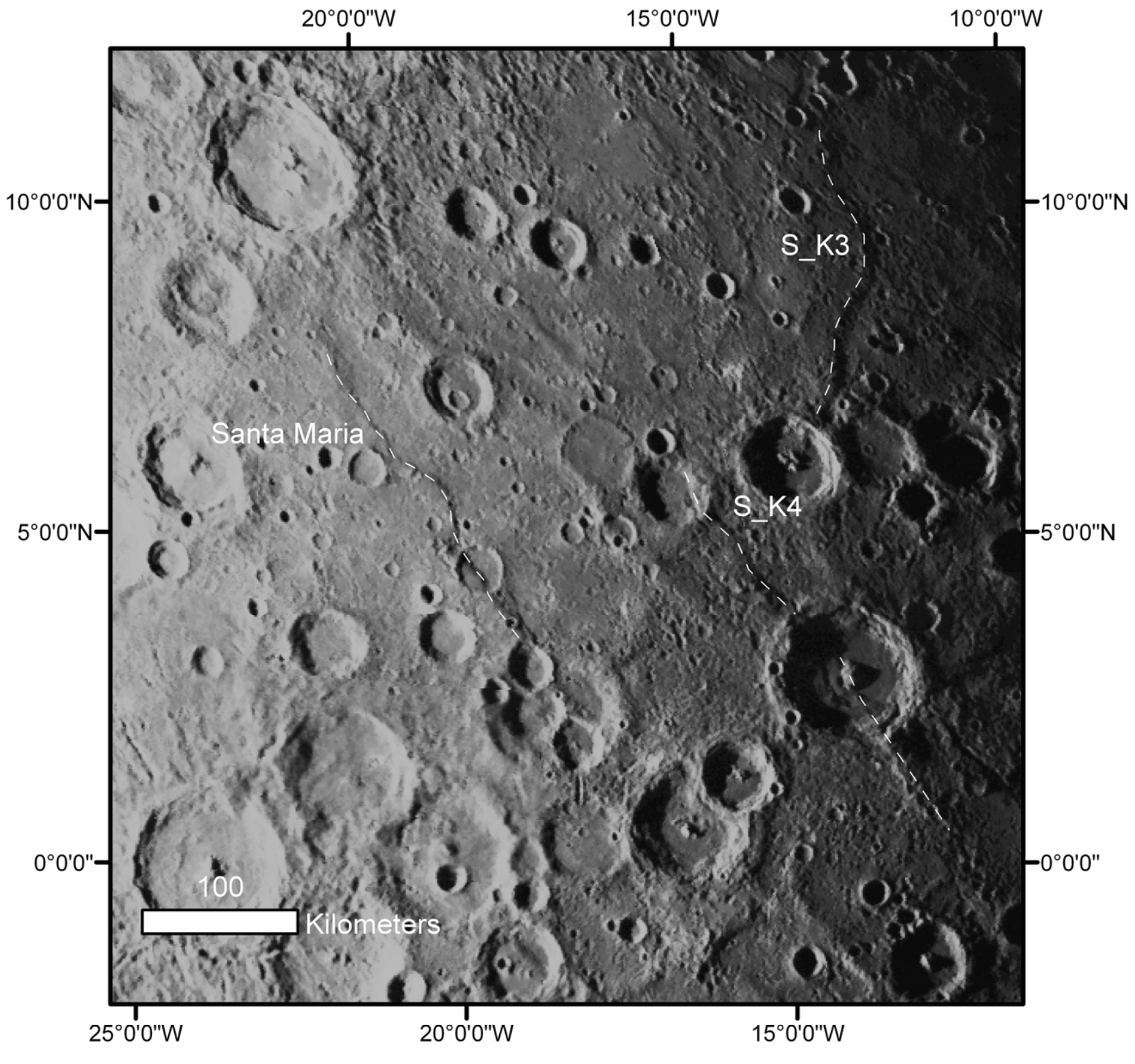
20°0'0"W
15°0'0"W
10°0'0"W
10°0'0"N
5°0'0"N
0°0'0"
25°0'0"W
20°0'0"W
15°0'0"W
S_K3
S_K4
Santa Maria
100
Kilometers

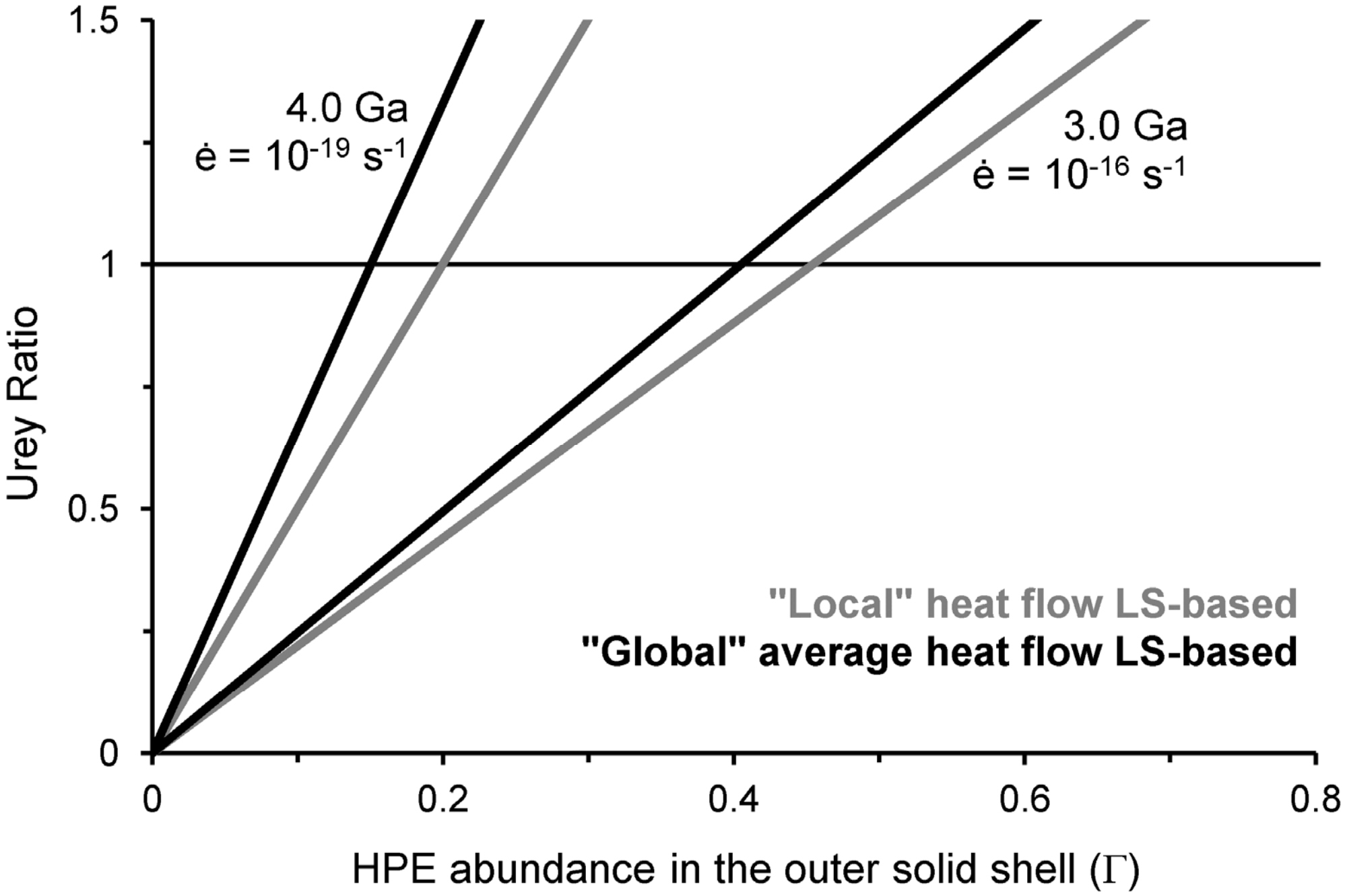
1.5
1
0.5
0
Urey Ratio
4.0 Ga
ė = 10-19 s-1
3.0 Ga
ė = 10-16 s-1
"Local" heat flow LS-based
"Global" average heat flow LS-based
0
0.2
0.4
0.6
0.8
HPE abundance in the outer solid shell (Γ)

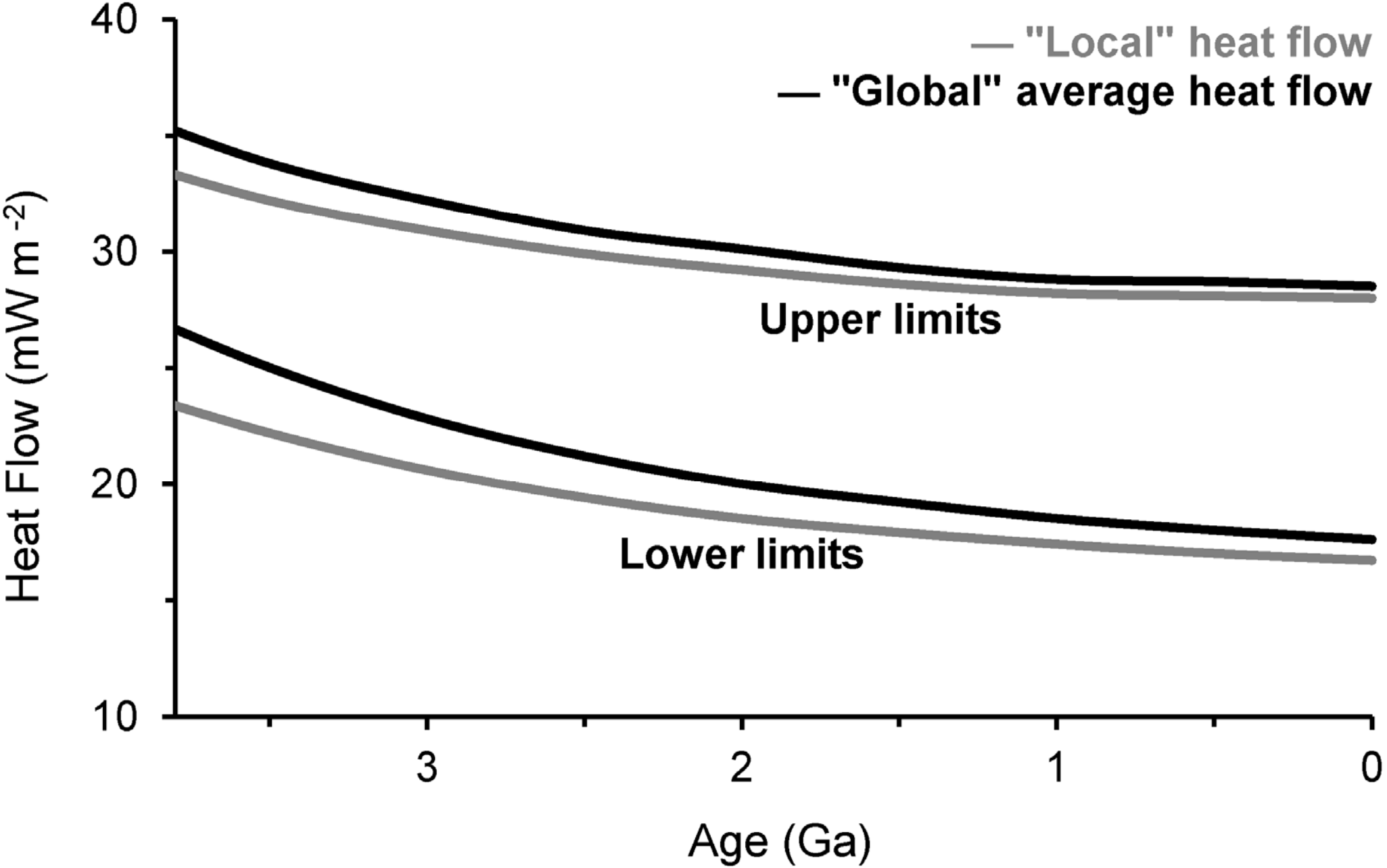
40
30
20
10
Heat Flow (mW m -2)
3
2
1
0
Age (Ga)
— "Local" heat flow
— "Global" average heat flow
Upper limits
Lower limits

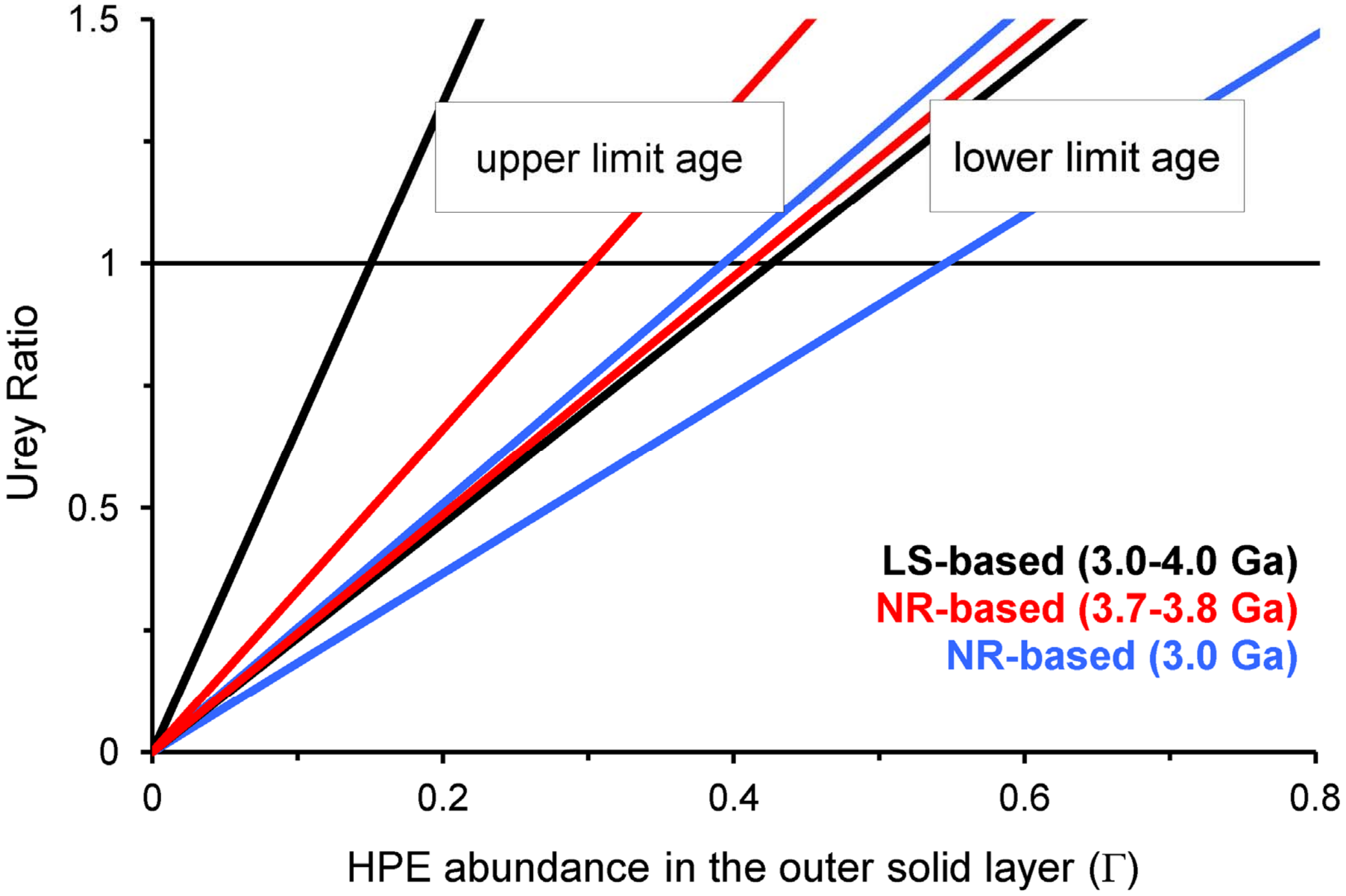
1.5
1
0.5
0
Urey Ratio
upper limit age
lower limit age
LS-based (3.0-4.0 Ga)
NR-based (3.7-3.8 Ga)
NR-based (3.0 Ga)
0
0.2
0.4
0.6
0.8
HPE abundance in the outer solid layer (Γ)